RESEARCH ARTICLE

Systematic Study on Swelling/Delamination of Layered Metal Oxides with Quaternary Ammonium Ions: Production of Well-Shaped/Oversized Unilamellar Nanosheets

Yeji Song,[a,b] Nobuyuki Sakai,[a] Yasuo Ebina,[a] Nobuo Iyi,[a] Takayuki Kikuchi,[a] Renzhi Ma,[a] Yasuhiro Ishida,[c] and Takayoshi Sasaki*[a,b]

[a] Dr. Y. Song, Dr. N. Sakai, Dr. Y. Ebina, Dr. N. Iyi, T. Kikuchi, Prof. R. Ma, Prof. T. Sasaki
Research Center for Materials Nanoarchitectonics (MANA)
National Institute for Materials Science (NIMS)
1-1 Namiki, Tsukuba, Ibaraki 305-0044, Japan
E-mail: sasaki.takayoshi@nims.go.jp

[b] Dr. Y. Song, Prof. T. Sasaki
Materials Science and Engineering, Graduate School of Pure and Applied Sciences
University of Tsukuba
1-1-1 Tennodai, Tsukuba, Ibaraki 305-8577, Japan

[c] Dr. Y. Ishida
RIKEN Center for Emergent Matter Science
2-1 Hirosawa, Wako, Saitama 351-0198, Japan

Supporting information for this article is given via a link at the end of the document.

Abstract: Enormous swelling of layered host compounds in an aqueous solution of various amines has been investigated as an important step in the synthesis of molecularly thin 2D nanosheets. However, a complete understanding of the reaction process has not been attained, which is the barrier for producing high-quality unilamellar nanosheets. Here, the swelling and delamination behaviors of platelet single crystals of protonated layered metal oxides are systematically examined with a series of tetraalkylammonium (TAA) hydroxide solutions. Upon contact with the solutions, the crystals immediately underwent massive expansion by several tens to hundreds of times. The swollen crystals can be delaminated into elementary layers by the application of external shear force. The exfoliation behavior is dependent on TAA ions, especially in terms of yield and lateral size/shape of the delaminated nanosheets. The swollen crystals with TAA ions with longer alkyl chains are delaminated almost completely, but irregular and fractured small sheets are yielded. Such long alkyl chains become entangled on the oxide layer and resulting hydrophobic interactions may be responsible for the lateral fragmentation. It is found that replacement of aqueous solutions with organic solvents to suppress the hydrophobic interactions is effective to produce oversized nanosheets in rectangular shape with sharp edges.

1. Introduction

In the past decades, molecularly thin 2D nanomaterials, or nanosheets, have received enormous attention due to their wide range of intriguing functionalities.[1-3] Nanosheets of various compositions and structures, such as graphene, nitrides, carbides, chalcogenides, halides, oxides, and hydroxides, have been synthesized using different methods based on the nature of the 2D materials. One of the most important and powerful methods is the disintegration of layered hosts into their elementary single layers. Mechanical cleavage has been applied mainly to van der Waals (vdW) layered compounds, which are characterized by rather weak interlayer interactions. The isolation of graphene from graphite crystals by peeling it off with adhesive tape is a well-known and typical example.[4,5] Besides the vdW compounds, there are a variety of layered hosts, such as metal oxides, phosphates, clay minerals, and hydroxides, which accommodate ion-exchangeable ions in the interlayer space.[6,7] The host layers are electrically charged and tightly held together by electrostatic interaction. In addition to the above compounds, transition metal chalcogenides derived by reductive intercalation with alkali metal ions, typically Li_xMoS_2, can be included in these classes of compounds.[8] Various effective methods for delaminating these compounds have been developed by utilizing the ion-exchange reactivities, and a range of novel properties have been reported in the resulting 2D nanosheets. The general delamination procedures involve the insertion of some bulky guest species to expand the interlayer galleries, loosening the binding force between the layers. In particular, small-sized alkali metal ions (Li^+, Na^+) with high hydration energy and various amines/organoammonium ions are found effective to induce very high degrees of interlayer swelling via permeation of electrolyte solutions.[9-24] Such so-called osmotic swelling has been studied on various layered compounds in polycrystalline form, revealing that their gallery height can reach up to 100 times the original value before the reaction, typically ~1 nm. Recently, platelet crystals of several tens of micrometers in size have been synthesized to study their swelling behaviors in more depth and to produce large-sized high-quality nanosheets.[25-30] Interestingly, massive accordion-like swelling has been directly observed under

the optical microscope, providing deep insights into the intriguing reactions.

Applying an external force to such a highly swollen sample in a solution can make layers fall apart. Since the interlayer galleries of the layered compounds are equivalent in reactivity, the massive interlayer expansion occurs uniformly across the crystals. Thus, in principle, disintegration into individual elementary layers is facilitated to produce a colloidal suspension, in which a large number of unilamellar nanosheets are dispersed. This is an obvious advantage over the mechanical cleavage method, which has drawbacks in terms of limited yield and low reproducibility/controllability, hampering practical applications. Although this process induced by intercalation/ion exchange of layered compounds is highly effective in producing their 2D nanosheets, a full understanding of the delamination behavior has not yet been attained. For example, although many delaminating agents have been used, it is not clear which is the most effective, what the differences are in terms of the quality of the resulting nanosheets (size, shape, yield, crystallinity, etc.), what the chemical action of each agent is, and so on. Quaternary ammonium ions, typically tetrabutylammonium (TBA) ion, are known to be one of the most effective reagents. In addition to the TBA ion, there are a series of tetraalkylammonium (TAA) ions, e.g., TMA, TEA, TPA, and TBA (-methyl-, -ethyl-, -propyl-, and -butyl-, respectively), which provide an ideal stage for studying swelling/exfoliation reactions against progressively varying size/chemical nature of delaminating agents (Figure S1). However, such a study has been limited to date.

It has been reported that polycrystalline powder samples of layered metal oxides, such as $Cs_{0.7}Ti_{1.825}\square_{0.175}O_4$ (□: vacancy), $K_{0.8}Ti_{1.73}Li_{0.27}O_4$, and $KCa_2Nb_3O_{10}$, can undergo delamination into corresponding single layers upon the action of TBA ions and related agents.[17-19,31,32] Resulting unilamellar nanosheets of $Ti_{1-\delta}O_2^{4\delta-}$ and $Ca_2Nb_3O_{10}^-$ exhibit fascinating functionalities, including high-κ dielectricity, photocatalytic activity, and serving as seed layers for heteroepitaxial film growth.[31,33-44] These properties hold promise for potential applications in the fields of electronics, catalysis, and energy conversion. To achieve these applications, the production of high-quality nanosheets is crucial. Therefore, a comprehensive understanding of the swelling/delamination reaction processes, especially in large-sized crystals, is essential.

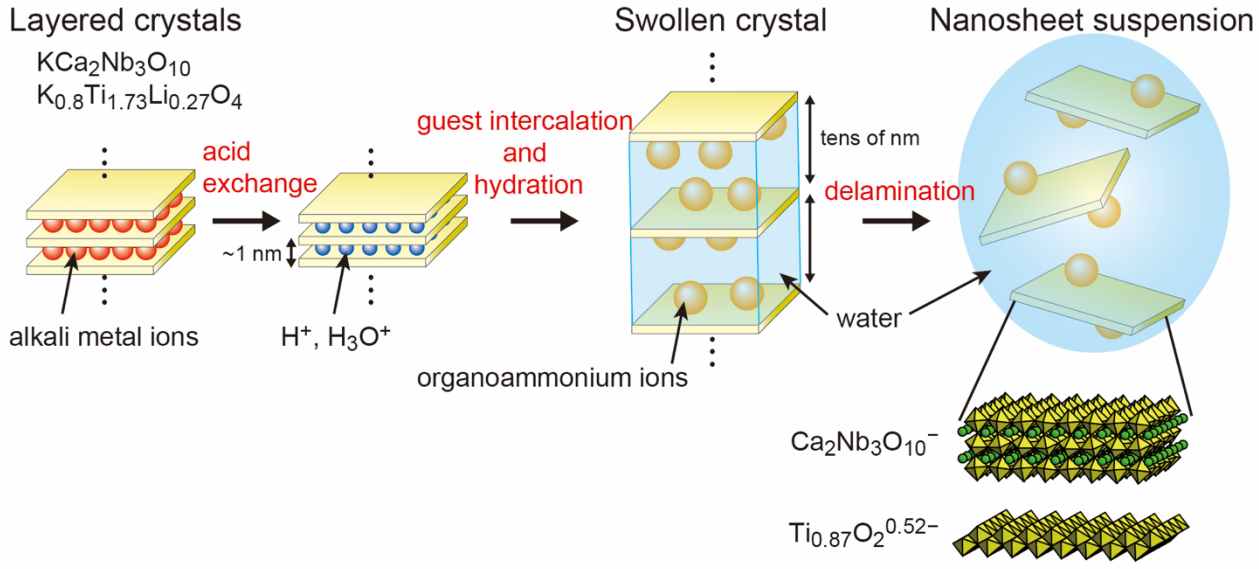

Scheme 1. Schematic diagram illustrating the hydration-driven swelling of layered crystals and exfoliation into unilamellar nanosheets.

In this study, we have systematically examined the swelling/delamination behavior of flux-grown crystal samples of these layered metal oxides upon contact with aqueous solutions of four TAA ions (Scheme 1). It was found that the lateral size of the obtained nanosheets and the exfoliation yield were strongly influenced by the guest species, suggesting that the coverage of the oxide layers with TAA ions and the hydrophobic interaction between adjacent ions are the key for the delamination behaviors. The findings in this study provide a clue to produce oversized high-quality nanosheets.

2. Results and Discussion

2.1. Swelling Behaviors of Layered Crystals

Single crystal samples of $KCa_2Nb_3O_{10}$ were synthesized through the flux-mediated growth and subsequently converted into $HCa_2Nb_3O_{10}\cdot 1.5H_2O$ via an acid-exchange process (Figure S2).[27] Platelet crystals within a size range of 25−53 μm were collected via sieving for the swelling/exfoliation study. The crystal thickness ranged from 5 to 20 μm (Figure S3), corresponding to a stack of 3000−12000 layers, considering the basal spacing of 1.63 nm.

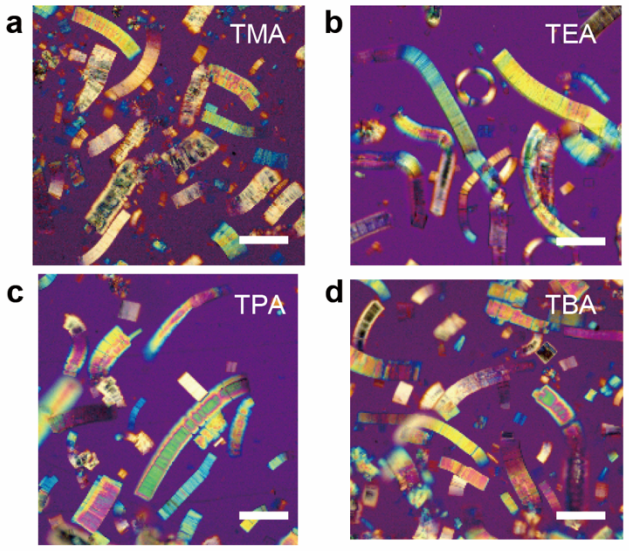

Figure 1. Polarized optical microscopy images of the swollen crystals of $HCa_2Nb_3O_{10}\cdot 1.5H_2O$ in a) TMAOH, b) TEAOH, c) TPAOH, and d) TBAOH solutions. The scale bars indicate 100 μm.

The obtained crystals of $HCa_2Nb_3O_{10}\cdot 1.5H_2O$ were immersed into a TAAOH solution at various concentrations. Significant expansion of the sample volume was readily observed within seconds, indicating macroscopic swelling in the solutions. Optical microscope observation revealed that the platelet crystals exhibited significant uniaxial elongation along the stacking direction of the host layers into a worm-like shape, as shown in Figure 1. The swollen crystals reached lengths of several hundred micrometers, indicating massive swelling up to ~100 folds, although shorter pieces were occasionally observed primarily due to the broad distribution of the initial crystal thickness. Small-angle X-ray scattering (SAXS) data displayed basal diffraction peaks of the swollen crystals (Figure S4), indicating very high degrees of swelling. The interlayer separation changed from ~20 to >100 nm (Figure 2a), depending on the TAA concentration, but was hardly dependent on the type of TAA ions. The degree of swelling was similar for all TAA ions as long as the same concentration was applied.

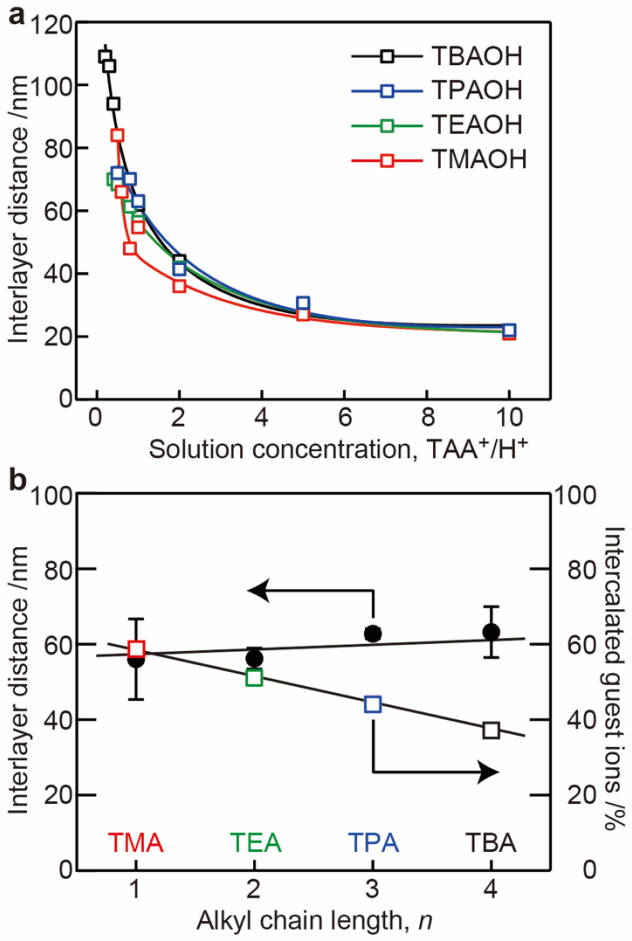

Figure 2. a) Interlayer distance of swollen crystals of $HCa_2Nb_3O_{10}\cdot 1.5H_2O$ in TMAOH, TEAOH, TPAOH, and TBAOH solutions at various concentrations (indicated by a molar ratio between the TAA ions applied and the exchangeable protons in the crystals. b) Interlayer distance and uptake of TAA ions when the corresponding hydroxide solutions were reacted with $HCa_2Nb_3O_{10}\cdot 1.5H_2O$ crystals at $TAA^+/H^+ = 1$.

The observed massive elongation of crystals originates from the homogeneous interlayer expansion via penetration of a large volume of the TAA solutions.[27] In this study, we focus on the swollen crystals obtained under conditions where the TAA molar dose was equivalent to that of exchangeable protons in the crystals. The obtained swollen crystals exhibited the interlayer spacing of 56−63 nm (Figure 2b), corresponding to a 30−40 folds expansion relative to the original basal spacing of platelet crystal of $HCa_2Nb_3O_{10}\cdot 1.5H_2O$. The degree of swelling was virtually comparable to each other for the TAA ions, as mentioned above. The intercalated amount of TAA ions was determined by acid-base titration, revealing that the uptake was 40%−60% of the exchangeable protons in the crystals (Figure 2b). The gradual decrease in uptake from TMA to TBA may be ascribed to steric effects.

2.2. Exfoliation Behaviors

The highly swollen crystals can be disintegrated into molecularly thin single layers when subjected to external shearing forces. Studying the delamination behaviors of these swollen crystals with the TAAOH solutions, which exhibit comparable extents of swelling, is of significant interest. One might expect similar exfoliation behaviors given their comparable degree of swelling. However, the results were contrary to this simple expectation, as described below.

The samples equilibrated with TAA solutions consisted of a top transparent solution and pasty swollen crystals sedimented at the bottom of the flask (see Figure 3). After mechanical shaking for 24 h, the swollen crystals with TPA and TBA ions totally transformed into turbid colloidal suspensions. Only a very small amount of sediments was observed even after standing overnight. In contrast, the samples with TMA and TEA ions displayed a translucent solution at the top and a sediment at the bottom. Observations under a polarized optical microscope indicated that the sediment was composed of swollen crystals, albeit with shorter lengths (Figure S5), suggesting that the elongated crystals were broken into shorter pieces.

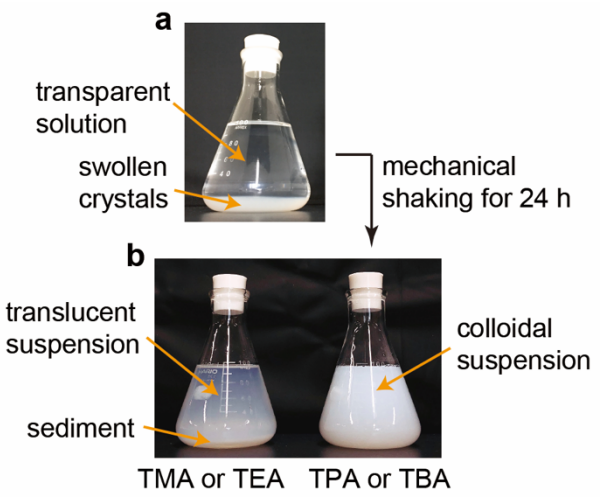

Figure 3. Photographs of a) swollen crystals of $HCa_2Nb_3O_{10}\cdot 1.5H_2O$ equilibrated with TAA solutions and b) samples after mechanical shaking.

Because the nanosheets exhibit intense optical absorption at 300 nm and below, UV-vis absorption spectra of their suspensions were measured to estimate the exfoliation yields for the samples containing the four TAA ions. As illustrated in Figure 4a, a noticeable difference in absorbance was observed between two groups: Group 1 (TMA and TEA) exhibited very low absorbance, while Group 2 (TPA and TBA) displayed much higher absorbance. The absorbance at 265 nm was converted to the exfoliation yield using the molar extinction coefficient (ε = 2.46 × 10^4 mol^{-1} dm^3 cm^{-1}, Supporting Information). As depicted in Figure 4b, the extent of exfoliation of the TPA and TBA samples (Group 2) was 92% after one day of mechanical shaking. In contrast, the yields for the TMA and TEA samples (Group 1) were only 3% and 9%, respectively. These low yields are consistent with a large amount of the sediments observed in these samples.

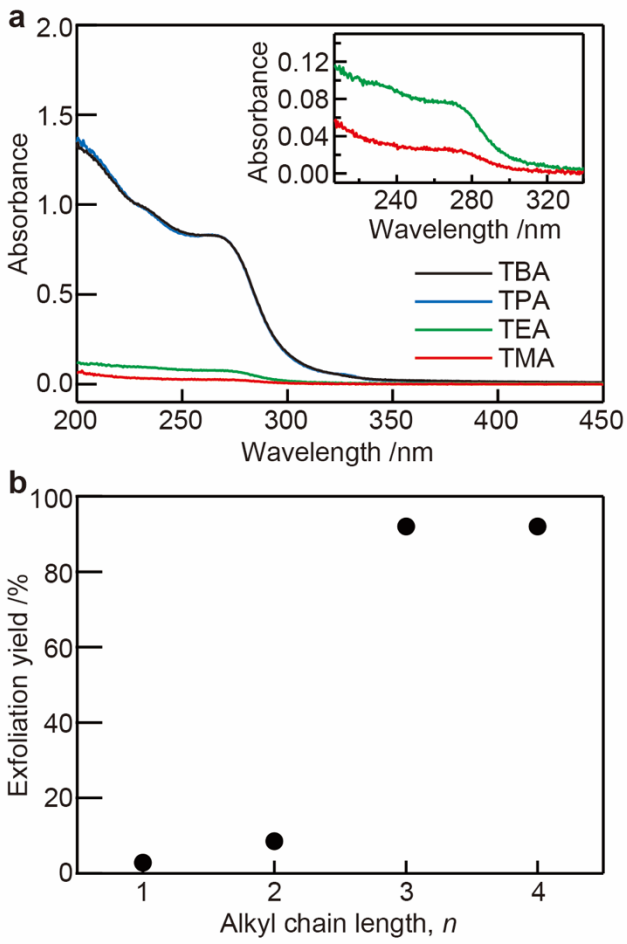

Figure 4. a) UV-vis absorption spectra of $Ca_2Nb_3O_{10}^-$ nanosheet suspensions. The inset shows expanded plots of TMA and TEA samples. b) The exfoliation yields calculated from the absorbance at 265 nm.

Droplets of the suspensions from the swollen crystals with different TAA solutions were dried on a cleaned surface of Si wafer, which was observed by atomic force microscopy (AFM). Figure 5a-d shows representative images, detecting ultrathin 2D nanosheets. A unique thickness of 1.8 nm, consistent with previously reported values for unilamellar $Ca_2Nb_3O_{10}^-$ nanosheets,[35] was observed for all the samples. However, it is important to note that the lateral size of the nanosheets varied significantly dependent on the reagents used (Figure S6). The nanosheets produced with TMA and TEA solutions exhibited an average lateral width of 8 μm, while delamination with TPA and TBA, which have longer alkyl chains, resulted in much smaller nanosheets with a lateral width of ~400 nm.

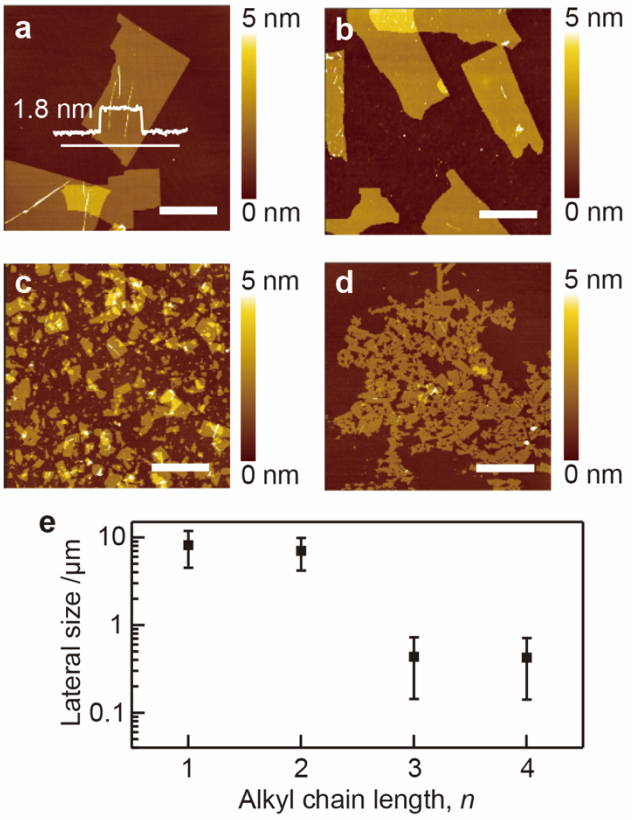

Figure 5. AFM images of $Ca_2Nb_3O_{10}^-$ nanosheets obtained in a) TMAOH, b) TEAOH, c) TPAOH, and d) TBAOH solutions. e) Average sizes of nanosheets in TAAOH solutions. The scale bars in AFM images measure 5 μm.

In summary, $Ca_2Nb_3O_{10}^-$ nanosheets with large lateral dimensions can be obtained by using aqueous solutions of smaller organoammonium ions, such as TMA and TEA, without severe fragmentation but in limited yields. These results suggest that crystals swollen with smaller ions are rather stable in aqueous media. On the other hand, the crystals swollen in TPA and TBA solutions were substantially delaminated (>90%), producing fragmented nanosheets.

Previous studies have investigated the massive swelling of the lepidocrocite-type layered titanates in various organoammonium and amine solutions.[25,26] However, delamination of such swollen crystals has not been reported. Therefore, we synthesized platelet crystals of $K_{0.8}Ti_{1.73}Li_{0.27}O_4$ using the flux-growth process, which were converted into the protonated form of $H_{1.07}Ti_{1.73}O_4{\cdot}H_2O$ (Figure S7).[45] The obtained crystals exhibited accordion-like elongation in TAAOH solutions, consistent with previous reports.[25,26] SAXS analysis indicates that the degree of swelling is not virtually dependent on TAA ions but is dominated by their concentrations. This trend parallels that observed for $HCa_2Nb_3O_{10}{\cdot}1.5H_2O$, as described above, as well as our previous study on isomorphous titanate crystals of $H_{0.8}Ti_{1.2}Fe_{0.8}O_4{\cdot}H_2O$.[25,26] In this study, we examined delamination behaviors for swollen crystals of $H_{1.07}Ti_{1.73}O_4{\cdot}H_2O$ with an interlayer spacing of ~40 nm, obtained at a reaction condition of TAA^+/H^+ = 1, in order to gain a deeper understanding by comparing these two typical layered systems, $H_{1.07}Ti_{1.73}O_4{\cdot}H_2O$ and $HCa_2Nb_3O_{10}{\cdot}1.5H_2O$.

Figure S8 depicts the swollen crystals of $H_{1.07}Ti_{1.73}O_4{\cdot}H_2O$ and the samples after shaking for 24 h. Similar to the trend observed for $HCa_2Nb_3O_{10}{\cdot}1.5H_2O$, crystals swollen with TPA and TBA ions were completely transformed into colloidal suspensions, whereas those swollen with TMA and TEA ions formed a colloidal top suspension with sediment at the bottom. The sediment observed in samples with TMA and TEA ions was smaller in amount compared to cases involving $HCa_2Nb_3O_{10}{\cdot}1.5H_2O$, indicating a higher degree of exfoliation. Their UV-vis absorption spectra revealed that the extent of delamination increased with the size of TAA ions (Figure S9). AFM observations confirmed the formation of unilamellar sheets of $Ti_{0.87}O_2^{0.52-}$ with a thickness ranging from 1.0 to 1.2 nm, and their lateral size decreased with increasing the ionic size (Figure S10), consistent with our previous report.[19] These trends mirror those observed in the delamination of $HCa_2Nb_3O_{10}{\cdot}1.5H_2O$, suggesting a common tendency among layered host compounds.

2.3. Lateral Fracture of the Oxide Sheets

The obtained nanosheets, both $Ca_2Nb_3O_{10}^-$ and $Ti_{0.87}O_2^{0.52-}$, clearly experienced the lateral fracture during the delamination process. Fragmentation was particularly significant for swollen crystals with TPA and TBA ions, while less pronounced for those with TMA and TEA. Based on the observed sizes of starting crystals and resulting nanosheets, it is estimated that one layer was cracked into ~10000 fragments for TBA, while fewer than 100 pieces for TMA. One straightforward assumption to explain such a notable difference is due to some mechanical stress, which may be imposed to the host layers in the initial stage of intercalation of these bulky ions. Although the well-expanded structure resulted upon equilibration with the TAA solutions, it is expected that swelling initiates by squeezing of large guests, particularly such as TPA and TBA ions, into the narrow interlayer gallery. The interlayer spacing of $HCa_2Nb_3O_{10}{\cdot}1.5H_2O$ and $H_{1.07}Ti_{1.73}O_4{\cdot}H_2O$ is 1.63 and 0.91 nm, respectively. The crystallographic thickness of the host layers is estimated as 1.44 and 0.70 nm, meaning that the net clearance is ~0.2 nm. This dimension is much smaller than the size of TPA and TBA ions, and severe deformation of the host layers is expected upon their penetration. On the other hand, such mechanical stress might be lighter for smaller ions such as TMA and TEA ions.

To examine the validity of this hypothesis, we carried out the following experiments for $HCa_2Nb_3O_{10}{\cdot}1.5H_2O$. The large nanosheets (~8 μm), obtained via exfoliation in the TMAOH solution, were sedimented upon centrifugation at 10000 rpm (10300 g) for 30 min and the top supernatant solution was discarded. Then, the sedimented nanosheets were redispersed into an equal volume of TBAOH solution. This process was repeated three times to ensure the replacement of TMA to TBA ions. To confirm the ion exchange, a few drops of the resulting suspension were dried on a glass slide, and its XRD data was recorded (Figure 6a). The sample showed a diffraction peak with a *d*-spacing of 2.50 nm. When dried, the nanosheets were generally restacked to yield a lamellar structure to accommodate guest species, which were present as counterions in the

suspension. In the control experiments, the dried samples from the nanosheets in TMAOH and TBAOH solutions showed peaks at 2.24 and 2.55 nm, respectively. The latter is very close to the value for the sample after the repeated replacement, strongly suggesting the substantial replacement of TBA for TMA ions by the procedure indicated above. Furthermore, FT-IR absorption spectra on the dried samples also support for the successful replacement (Figure S11). The absorption bands observed in a range of 3000−2800 cm^{-1} are attributed to stretching vibrations of $-CH_2-$ and $-CH_3$ groups.[46] The dried sample obtained from the suspension after repeating the solution replacement showed these peaks in comparable absorbance to the sample from the nanosheet suspension with TBAOH solution. On the other hand, the bands were very weak for the sample with TMA ions due to the much smaller alkyl group.

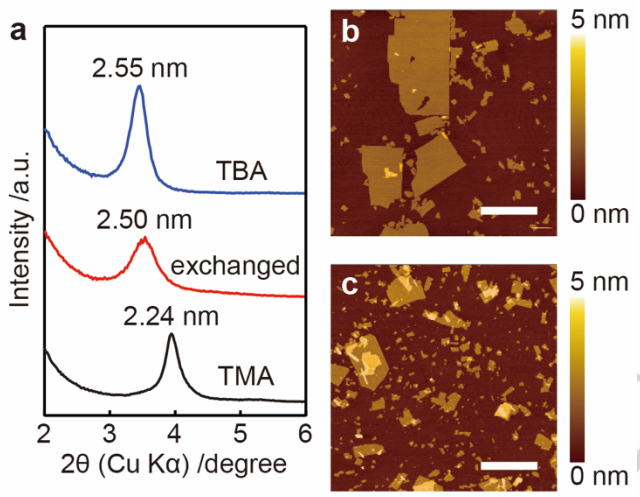

Figure 6. a) XRD patterns of restacked nanosheets after changing from the TMAOH solution to the TBAOH solution (red), as well as those from each solution (blue and black). For restacking, several drops of the suspension were dried on a glass slide in N_2 atmosphere, and XRD data were collected under N_2 gas flow. b,c) AFM images of nanosheets obtained from the TBAOH solution after changing from TMAOH before and after the shaking, respectively. Scale bar on AFM images indicates 5 μm.

Interestingly, the nanosheets started to undergo lateral fracture once counterions in the suspension were exchanged from TMA to TBA ions. As illustrated by AFM images in Figure 6b, it is evident that small sheets started to form. Furthermore, fragmentation was accelerated when mechanical shaking was applied. The nanosheets became smaller after shaking for 24 h (Figure 6c). The degree of fragmentation was similar to that in the direct exfoliation of swollen crystals in TBAOH solution. For comparison purposes, we also performed the same observation with a sample in which the supernatant was exchanged with TMAOH solution instead of the TBAOH solution. In this control sample, no change in lateral size was observed even after shaking for 24 h (Figure S12). These results clearly indicate that neither the mechanical stress caused at the moment of bulky ion (TBA and TPA) intercalation nor the mechanical agitation of the nanosheet suspensions is responsible for the lateral fracture of oxide layers.

2.4. Structural Considerations

To gain insights into the origin of different exfoliation behaviors, particularly the fragmentation of the nanosheets, structural aspects of swollen crystals are discussed. As mentioned above, the uptake of TAA ions into the crystals was estimated by the acid-base titration (Figure 2b). When the crystals were highly expanded, it is reasonable to expect that a majority of the ions are situated on the oxide surface, forming the so-called Stern layer, while a small fraction of them diffuses into the interlayer space.[47] Here we discuss about how the oxide layer surface is covered with TAA ions, ignoring the ions in such an electric double layer due to their small abundance. Figure 7 illustrates the top view of the $Ca_2Nb_3O_{10}^-$ layer, in which the 2D square lattice ($S_{unit\ cell}$: 0.386 × 0.386 nm^2)[44] is indicated. Since this 2D unit cell area has one negative charge, we can calculate the area occupied by one TAA ions, S, as $S = 2S_{unit\ cell}/x$, where x denotes the percent uptake value with respect to the theoretical ion-exchange capacity as depicted in Figure 2b. TAA ions ideally have a sp^3 bonding configuration (Figure S1). If we assume that TAA ions are situated on the surface of the oxide sheet in the typical orientation, namely, with the C_2 axis perpendicular to the 2D surface, as illustrated in Figure 7, we can estimate the projected area of the ions. By comparing these values with the occupied area calculated (Table S1), we can estimate the packing density and the distance between the ions, which indicate a clear distinction between Group 1 (TMA, TEA) and Group 2 (TPA, TBA) as mentioned above. For the former, the occupied areas are larger than the projected size of ions, indicating that the ions are situated on the oxide surface allowing some gaps between the ions. On the other hand, for the latter ions, the occupied areas are smaller than the ion size, and alkyl chains from the neighboring ions are intertangled.

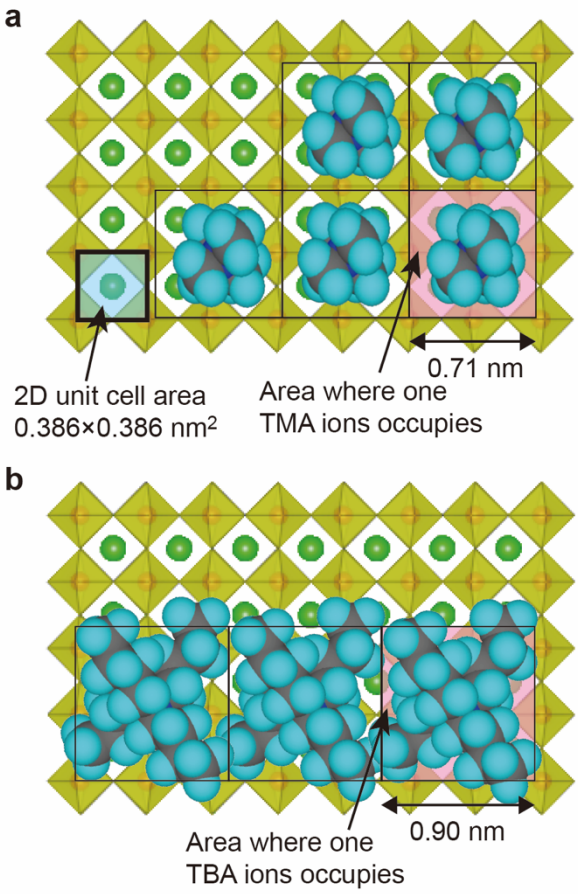

Figure 7. Schematic illustrations of adsorbed a) TMA and b) TBA ions on the host layer of $Ca_2Nb_3O_{10}^-$. TMA ions are isolated from neighboring ions, while TBA ions are in contact to each other.

A similar feature was found in the layered titanate, $H_{1.07}Ti_{1.73}O_4 \cdot H_2O$, which has a different layer architecture with a 2D rectangular unit cell of 0.3786 × 0.2983 nm^2.[48] We studied the swelling reactions in the TMA and TBA solutions, which resulted in the replacement of 34% and 28% of exchangeable protons, respectively, at the equivalent dose of TAA ions. Then the area occupied by one TAA ions is calculated to be 0.621 and 0.754 nm^2. The former is larger than the projection area of TMA ion, while the latter is smaller than that of TBA ion (Figure S13), the situation of which is the same with the case for $HCa_2Nb_3O_{10} \cdot 1.5H_2O$.

These aspects strongly suggest that the alkyl chains of TBA and TPA ions are interdigitated with those of neighboring ions, bringing about some intermolecular hydrophobic interaction. It is true that magnitude of such intermolecular force (~5 kJ mol^{-1}) is much smaller than the chemical bonds in the oxide nanosheets (~700 kJ mol^{-1}). However, owing to the molecularly thin 2D morphology, the cumulated intermolecular force over some area can surpass the chemical bond strength, which may eventually induce lateral fragmentation (Figure 8). Recently, we have reported that a similar scenario works in the scission of the nanosheets coated on a bumpy substrate surface.[48] The nanosheets are laterally cleaved along the fundamental crystallographic axes such as 10 and 01 to show the sharp edges.

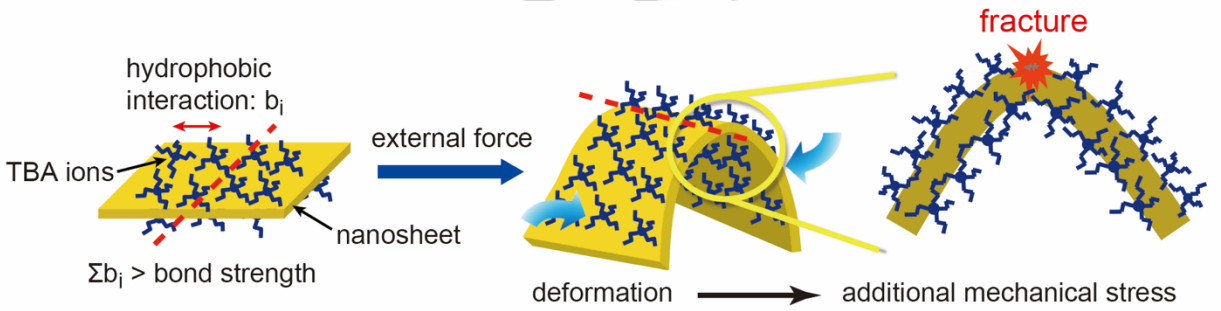

Figure 8. Schematic illustration of lateral fracture of nanosheets covered with TBA ions.

As described above, the fragmentation was accelerated upon agitation of the colloidal suspensions. Because the nanosheets are flexible enough to be bent when the suspension is shaken,[49-51] additional mechanical stress will be imposed onto the nanosheets, which provides a trigger for the lateral fracture of the nanosheets. On the other hand, smaller TMA and TEA ions are isolated from each other and do not have such interaction, leading to lesser degrees of fragmentation.

2.5. Delamination in Organic Solvents

Based on the above hypothesis to lateral fracture, we attempted to suppress the intermolecular interaction between TBA ions by exchanging the aqueous medium with some organic solvents. Various solvents were examined to find that dimethyl sulfoxide (DMSO) gave the best result. Recently, Breu et al. reported that clay minerals, specifically hectorite, effectively undergo delamination in polar and aprotic solvents including DMSO.[52-54] In our experiment, after inducing the hydration swelling of the crystals in the aqueous solution of TBAOH, the supernatant was decanted, and an equal volume of DMSO was added. The replacement process was repeated five times to ensure solvent exchange. No change in sample appearance was observed. Optical microscopy images indicated that the crystals in DMSO retained their highly elongated shape, confirming that the swollen

structure was preserved (Figure S14). Interestingly, the nanosheets obtained after 24 h of mechanical shaking were not broken into small pieces, which sharply contrasted with specimens in aqueous solutions. The obtained nanosheets had an average lateral size of 5−10 μm, as shown in AFM images (Figure 9a and b). Gentle manual shaking produced even larger sheets of over 20 μm (Figure 9c and d). Additionally, the nanosheets exhibited a rather rectangular shape with sharp facets, inherited from original platelet crystals. This result clearly indicates a much lesser degree of lateral fracture of the swollen crystals with TBA ions in DMSO, supporting the hypothesis that intermolecular hydrophobic interaction is associated with the fragmentation of the nanosheets. Because the hydrophobic interaction is weakened in organic solvents, the lateral fracture is largely suppressed as seen in Figure 9c, d. The UV-vis absorption spectrum of the DMSO suspension (Figure S15) revealed a moderate exfoliation yield of 25%. As described above, the delamination of swollen crystals with TMA ions in water could produce large-sized nanosheets, but the yield is low. Conversely, exfoliation of swollen sample with TBA ions in water could yield a higher percentage, yet resulting in small and irregularly shaped nanosheets. The present study reveals a delamination procedure capable of producing well-shaped nanosheets with large lateral dimensions through a facile route within a day.

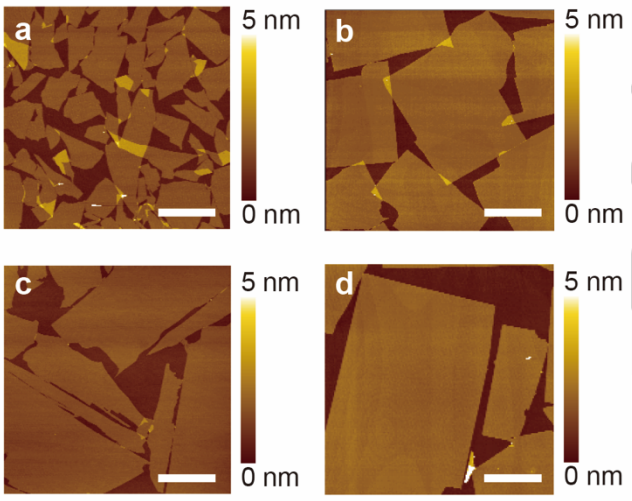

Figure 9. AFM images of nanosheets of a) $Ti_{0.87}O_2^{0.52-}$ and (b) $Ca_2Nb_3O_{10}^-$ exfoliated from swollen crystals with TBA ions via mechanical shaking in DMSO, and c,d) those correspondingly obtained by gentle agitation. The scale bars indicate 5 μm.

The swollen titanate crystals also remained unchanged when the aqueous media were changed to the organic solvents (Figure S16a). Larger-sized nanosheets were also produced when swollen titanate crystals with TBA ions were shaken in organic media (Figure S16b). Suppression of lateral fracture is evident, indicating the validity of the scenario associated with the role of intermolecular force.

3. Conclusion

The swelling and exfoliation behaviors of platelet crystals of the layered perovskite niobate and lepidocrocite-type titanate were systematically examined using four TAAOH solutions in terms of swelling degree, delamination yield, and the lateral size/quality of obtained nanosheets. Delamination in TMA- and TEAOH solutions produced unilamellar nanosheets with large lateral dimensions, but the yield was rather limited. On the other hand, swollen crystals in TPA- and TBAOH solutions underwent total delamination, but the resulting sheets were much smaller and irregular in shape. The exfoliation behaviors are distinctly different, even despite comparable swelling extents of layered crystals with all kinds of TAAOH solutions employed. We have revealed that such exfoliation features may be correlated with the intermolecular interaction between TAA ions adsorbed on the nanosheets. Smaller ions such as TMA and TEA are isolated from each other on the oxide layer, while larger TPA and TBA ions are intertangled. The intermolecular interaction between them may be the origin for lateral fracture of 2D oxide nanosheets. Square-shaped nanosheets in lateral dimensions over 10 μm were facilely obtained by delaminating the swollen crystals in organic solvents, which can suppress the intermolecular interaction. This study sheds light on the overlooked chemical roles of delaminating agents of the layered crystals, the understanding of which is helpful for the controlled synthesis of high-quality 2D nanomaterials. This swelling/delamination process is expected to be applicable to various classes of layered host compounds accommodating interlayer counter ions, e.g., layered metal oxides, chalcogenides (reduced form), phosphates, clay minerals, and layered zeolites.

Acknowledgements

This work was supported by the World Premier International Research Center Initiative (WPI), MEXT, Japan, and CREST of the Japan Science and Technology Agency (JST) (grant no. JPMJCR17N1 & JPMJCR22B1), Japan. The authors were grateful to Prof. Nobuyoshi Miyamoto (Fukuoka Institute of Technology) for help in SAXS measurements.

Keywords: Delamination • Hydrophobic effect • Intercalation • Layered compounds • Oversized high-quality nanosheets

[1] R. Ma. T. Sasaki, *Adv. Mater.* **2010**, *22*, 5082.

[2] S. Z. Butler, S. M. Hollen, L. Cao, Y. Cui, J. A. Gupta, H. R. Gutiérrez, T. F. Heinz, S. S. Hong, J. Huang, A. F. Ismach, E. Johnston-Halperin, M. Kuno, V. V. Plashnitsa, R. D. Robinson, R. S. Ruoff, S. Salahuddin, J. Shan, L. Shi, M. G. Spencer, M. Terrones, W. Windl, J. E. Goldberger, *ACS Nano* **2013**, *7*, 2898.

[3] V. Nicolosi, M. Chhowalla, M. G. Kanatzidis, M. S. Strano, J. N. Coleman, *Science* **2013**, *340*, 1226419.

[4] K. S. Novoselov, A. K. Geim, S. V. Morosov, D. Jiang, Y. Zhang, S. V. Dubonos, I. V. Grigorieva, A. A. Firsov, *Science* **2004**, *306*, 666.

[5] A. K. Geim, K. S. Novoselov, *Nat. Mater.* **2007**, *6*, 183.

[6] A. Clearfield, *Chem. Rev.* **1988**, *88*, 125.

[7] R. Uppuluri, A. Sen Gupta, A. S. Rosas, T. E. Mallouk, *Chem. Soc. Rev.* **2018**, *47*, 2401.

[8] R. Schöllhorn, *Intercalation Chemistry* (Eds.: M. S. Whittingham, A. J. Jacobson), Academic Press, New York, **1982**, pp 315–360.

[9] K. Norrish, *Nature* **1954**, *173*, 256.

[10] W. G. Garrett, G. F. Walker, *Clays Clay Miner.* **1960**, *9*, 557.

[11] G. F. Walker, W. G. Garrett, *Nature* **1961**, *191*, 1389.

[12] L. F. Braganza, R. J. Crawford, M. V. Smalley, R. K. Thomas, *Clays Clay Miner.* **1990**, *38*, 90.

[13] P. Joensen, R. F. Frindt, S. R. Morrison, *Mater. Res. Bull.* **1986**, *21*, 457.

[14] M. M. J. Treacy, S. B. Rice, A. J. Jacobson, J. T. Lewandowski, *Chem. Mater.* **1990**, *2*, 279.

[15] H.-N. Kim, S. W. Keller, T. E. Mallouk, *Chem. Mater.* **1997**, *9*, 1414.

[16] M. Zhao, C. Casiraghi, K. Parvez, *Chem. Soc. Rev*. **2024**, *53*, 3036.

[17] T. Sasaki, M. Watanabe, H. Hashizume, H. Yamada, H. Nakazawa, *J. Am. Chem. Soc.* **1996**, *118*, 8329.

[18] T. Sasaki, M. Watanabe, *J. Am. Chem. Soc.* **1998**, *120*, 4682.

[19] T. Maluangnont, K. Matsuba, F. Geng, R. Ma, Y. Yamauchi, T. Sasaki, *Chem. Mater.* **2013**, *25*, 3137.

[20] Z.-H. Liu, K. Ooi, H. Kanoh, W.-P. Tang, T. Tomida, *Langmuir* **2000**, *16*, 4154.

[21] Y. Omomo, T. Sasaki, L. Z. Wang, M. Watanabe, *J. Am. Chem. Soc.* **2003**, *125*, 3568.

[22] Z. Liu, R. Ma, M. Osada, N. Iyi, Y. Ebina, K. Takada, T. Sasaki, *J. Am. Chem. Soc.* **2006**, *128*, 4872.

[23] W. J. Roth, T. Sasaki, K. Wolski, Y. Song, D.-M. Tang, Y. Ebina, R. Ma, J. Gryzbek, K. Kalahurska, B. Gil, M. Mazur, S. Zapotoczny, J. Cejka, *Sci. Adv.* **2020**, *6*, eaay8163.

[24] W. J. Roth, T. Sasaki, K. Wolski, Y. Ebina, D.-M. Tang, Y. Michiue, N. Sakai, R. Ma, O. Cretu, J. Kikkawa, K. Kimoto, K. Kalahurska, B. Gil, M. Mazur, S. Zapotoczny, J. Cejka, J. Gryzbek, A. Kowalczyk, *J. Am. Chem. Soc.* **2021**, *143*, 11052.

[25] F. Geng, R. Ma, A. Nakamura, K. Akatsuka, Y. Ebina, Y. Yamauchi, N. Miyamoto, Y. Tateyama, T. Sasaki, *Nat. Commun.* **2013**, *4*, 1632.

[26] F. Geng, Y. Ebina, Y. Yamauchi, N. Miyamoto, T. Sasaki, *J. Am. Chem. Soc.* **2014**, *136*, 5491.

[27] Y. Song, N. Iyi, T. Hoshide, T. C. Ozawa, Y. Ebina, R. Ma, S. Yamamoto, N. Miyamoto, T. Sasaki, *Dalton Trans.* **2018**, *47*, 3022.

[28] M. Stöter, D. A. Kunz, M. Schmidt, D. Hirsemann, H. Kalo, B. Putz, J. Senker, J. Breu, *Langmuir* **2013**, *29*, 1280.

[29] S. Rosenfeldt, M. Stöter, M. Schlenk, T. Martin, R. Q. Albuquerque, S. Förster, J. Breu, *Langmuir* **2016**, *32*, 10582.

[30] G. Cha, S. Weiß, J. Thanner, S. Rosenfeldt, V. Dudko, F. Uhlig, M. Stevenson, I. Pietsch, R. Siegel, D. Friedlich, W. Bensch, J. Senker, N. Sakai, T. Sasaki, J. Breu, *Chem. Mater.* **2023**, *35*, 7208.

[31] R. E. Schaak, T. E. Mallouk, *Chem. Mater.* **2002**, *14*, 1455.

[32] Y. Ebina, T. Sasaki, M. Watanabe, *Solid State Ionics* **2002**, *151*, 177.

[33] J. E. ten Elshof, H. Yuan, P. G. Rodriguez, *Adv. Energy Mater.* **2016**, *6*, 1600355.

[34] M. Osada, Y. Ebina, H. Funakubo, S. Yokoyama, T. Kiguchi, K. Takada, T. Sasaki, *Adv. Mater.* **2006**, *18*, 1023.

[35] M. Osada, K. Akatsuka, Y. Ebina, H. Funakubo, K. Ono, K. Takada, T. Sasaki, *ACS Nano* **2010**, *4*, 5225.

[36] N. Sakai, K. Fukuda, T. Shibata, Y. Ebina, K. Takada, T. Sasaki, *J. Phys. Chem. B* **2006**, *110*, 6198.

[37] G. Liu, L. Wang, C. Sun, X. Yan, L. Cheng, H.-M. Cheng, G. Q. Lu, *Chem. Commun.* **2009**, 1383.

[38] J. L. Gunjakar, T. W. Kim, H. N. Kim, I. Y. Kim, S.-J. Hwang, *J. Am. Chem. Soc.* **2011**, *133*, 14998.

[39] O. C. Compton, E. C. Carroll, J. Y. Kim, D. S. Larsen, F. E. Osterloh, *J. Phys. Chem. C* **2007**, *111*, 14589.

[40] Y. Matsumoto, S. Ida, T. Inoue, *J. Phys. Chem. C* **2008**, *112*, 11614.

[41] K. Maeda, M. Eguchi, W. J. Youngblood, T. E. Mallouk, *Chem. Mater.* **2009**, *21*, 3611.

[42] K. Maeda, M. Eguchi, T. Oshima, *Angew. Chem. Int. Ed.* **2014**, *53*, 13164.

[43] K. Kikuta, K. Noda, S. Okumura, T. Yamaguchi, S. Hirano, *J. Sol-Gel Sci. Technol.* **2007**, *42*, 381.

[44] T. Shibata, K. Fukuda, Y. Ebina, T. Kogure, T. Sasaki, *Adv. Mater.* **2008**, *20*, 231.

[45] T. Sasaki, F. Kooli, M. Iida, Y. Michiue, S. Takenouchi, Y. Yajima, F. Izumi, B. C. Chakoumakos, M. Watanabe, *Chem. Mater.* **1998**, *10*, 4123.

[46] G. Socrates, *Infrared Characteristic Group Frequencies,* 2nd Ed., John Wiley & Sons Ltd., Chichester, **1980**, pp 34–41.

[47] M. Smalley, *Clay Swelling and Colloid Stability*, Taylor & Francis, Boca Raton, **2006**, pp 159–175.

[48] N. Sakai, M. Suzuki, T. Sasaki, *Adv. Mater. Interfaces* **2022**, *9*, 2102591.

[49] T. Nakato, Y. Higashi, W. Ishitobi, T. Nagashita, M. Tominaga, Y. Suzuki, T. Iwai, J. Kawamata, *Langmuir* **2019**, *35*, 5568.

[50] L. Z. Wang, T. Sasaki, Y. Ebina, K. Kurashima, M. Watanabe, *Chem. Mater.* **2002**, *14*, 4827.

[51] R. Ma, Y. Bando, T. Sasaki, *J. Phys. Chem. B* **2004**, *108*, 2115.

[52] V. Dudko, K. Ottermann, S. Rosenfeldt, G. Papastavrou, J. Breu, *Langmuir* **2021**, *37*, 461.

[53] V. Dudko, S. Rosenfeldt, R. Siegel, J. Senker, M. Matejdes, J. Breu, *Langmuir* **2022**, *38*, 10781.

[54] K. Imwiset, V. Dudko, P. Markus, G. Papastavrou, J. Breu, M. Ogawa, *Chem. Commun.* **2024**, *60*, 6383.

Entry for the Table of Contents

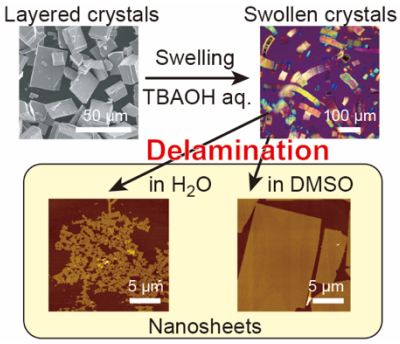

Oversized high-quality nanosheets can be obtained by delaminating layered crystals, swollen by tetrabutylammonium (TBA) hydroxide, in dimethyl sulfoxide (DMSO), whereas the delamination in water results in the fracture of the nanosheets due to hydrophobic interaction of entangled alkyl chains of neighboring TBA ions adsorbed on the nanosheets. The delamination in DMSO can weaken the hydrophobic interaction to suppress the fracture.

WILEY-VCH